Influence of atmospheric turbulence on the performance and design of GENIE

Olivier Absil[a], Roland den Hartog[b], Philippe Gondoin[b], Pierre Fabry[b], Luigi d'Arcio[b], Rainer Wilhelm[c], Philippe Gitton[c] and Florence Puech[c]

[a]Institut d'Astrophysique et de Géophysique, 17 Allée du Six Août, Liège, Belgium
[b]Science Payloads and Advanced Concepts Office, ESA/ESTEC, postbus 299, NL-2200 AG Noordwijk, The Netherlands
[c] European Southern Observatory, Karl-Schwarzschild-Str. 2, D-85748 Garching bei Muenchen, Germany

ABSTRACT

Two competitive design studies for the Ground-based European Nulling Interferometer Experiment (GENIE) have been initiated by the European Space Agency and the European Southern Observatory in November 2003.[1] The GENIE instrument will most probably consist of a two-telescope Bracewell interferometer, using the 8-m Unit Telescopes and/or the 1.8-m Auxiliary Telescopes of the VLTI, and working in the infrared L' band (3.5 – 4.1 μm). A critical issue affecting the overall performance of the instrument is its capability to compensate for the phase and intensity fluctuations produced by the atmospheric turbulence.[2] In this paper, we present the basic principles of phase and intensity control by means of real-time servo loops in the context of GENIE. We then propose a preliminary design for these servo loops and estimate their performance using GENIEsim, the science simulation software for the GENIE instrument.[3]

Keywords: Nulling interferometry, Darwin-GENIE, atmospheric turbulence, modeling, instrumentation, servo loops

1. INTRODUCTION

In the context of the Darwin Technical Research Programme, the European Space Agency has initiated two competitive definition studies for a ground-based nulling interferometer, lead by Alcatel Space and EADS Astrium. The main goal of this instrument is to test some of the key components and techniques of the Darwin space mission, such as achromatic phase shifters, mid-infrared single-mode fibers, delay lines, fringe sensors, detectors, cryogenics, ... GENIE will consist of a Bracewell interferometer formed of two VLT 8-m Unit Telescopes (UT) or 1.8-m Auxiliary Telescopes (AT) operating in the infrared L' band (3.5 – 4.1 μm).[1] It will validate on ground the concept of nulling interferometry and allow the European scientific community to build experience in the operation of a nulling interferometer and in its specific data analysis. Besides its technical goals, GENIE will also prepare the Darwin science programme by surveying nearby main-sequence stars for exozodiacal dust clouds at the level of 20 times our local zodiacal cloud. This will allow to cull the stars surrounded by too much dust, for which the exozodiacal emission becomes the main source of noise in the case of Darwin. These dust disks are typically 10^4 to 2×10^4 times fainter than their parent star in the L' band. In order to detect such faint disks with a high enough signal-to-noise ratio (typically: SNR > 5), GENIE needs to achieve calibrated nulling ratios of about 10^5.

GENIE, as a scientific instrument, will also help characterize the inner part of protoplanetary disks around young stars, where planet formation could be detected by the presence of gaps or disk asymmetries. An additional objective of GENIE is to detect the thermal emission from a few bright hot Jupiters and to perform low-resolution spectroscopy to characterize their atmospheres.

Further author information: (Send correspondence to O.A.)
O.A.: absil@astro.ulg.ac.be
R.d.H.: rdhartog@rssd.esa.int

2. PRINCIPLE OF NULLING INTERFEROMETRY

The principle of nulling interferometry is to combine the light beams collected by two or more telescopes in a co-axial way, adjusting the phases of the different beams in order to produce a destructive interference on the optical axis. This process strongly attenuates the light coming from the central bright object (e.g. star) while letting through the light from slightly off-axis sources such as planets, dust disks, etc. A nulling interferometer is characterized by its transmission map, illustrated in Fig. 1 in the case of a two-telescope interferometer ("Bracewell interferometer"[4]). The expression of the transmission map results from the superposition of the two-telescope interference fringe pattern onto the Airy pattern associated to a single pupil:

$$T(\theta,\phi) = 2\left(\frac{2J_1(\pi\theta d/\lambda)}{\pi\theta d/\lambda}\right)^2 \sin^2\left(\pi\tfrac{b\theta}{\lambda}\cos\phi\right) \ , \tag{1}$$

where b is the interferometer baseline and d the telescope diameter. It determines the regions of the field-of-view which are transmitted and those that are cancelled by the interference process. The flux recorded at the destructive output of the interferometer is computed by integrating the source distribution multiplied by the transmission map on the field-of-view.

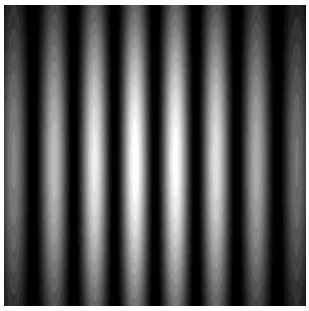

Figure 1. Transmission map in the L' band for a 50 m Bracewell interferometer formed of two 8-m telescopes. The interferometric field-of-view is 125 mas while the spacing between two successive bright fringes is 17 mas.

Assuming that there are no instrumental errors, the destructive interference achieved by the interferometer is perfect, but only on the optical axis. An extended object such as a stellar disk will thus not be perfectly cancelled by the nulling process. We define the *rejection rate* ρ as the ratio between the initial stellar flux at the input of the beam-combiner and the stellar flux transmitted by the nuller at the destructive output (referred to as "stellar leakage", and given by the 2D integral of the transmission map on the stellar disk):

$$\rho = \frac{2F_*\pi\theta_*^2}{\int_0^{\theta_*}\int_0^{2\pi} T(\theta,\phi)B_*(\theta,\phi)\theta \mathrm{d}\phi\mathrm{d}\theta} \ , \tag{2}$$

with F_* the stellar flux in Jy and B_* the stellar brightness in Jy/sr. Working out the integral by assuming that the stellar size is much smaller than the fringe spacing λ/b , one ends up with the following approximation:

$$\rho \simeq \frac{\pi^2}{4}\left(\frac{b\theta_*}{\lambda}\right)^2 \tag{3}$$

The expression (3) of the rejection rate is valid only for a perfect Bracewell interferometer. In practice, the rejection rate is degraded by imperfect co-phasing of the light beams, intensity mismatches and polarization errors.[5] The residual stellar signal at the output of the interferometer can thus be divided into two parts:

- The *geometric leakage*, proportional to $1/\rho$, is associated to the finite size of the stellar disk and depends on the length of the interferometer baseline. Calibration techniques such as precise measurements of stellar diameters can be used to reduce this contribution down to an acceptable level (10^{-5} of the initial stellar flux).

- The *instrumental leakage*, which is produced by the effects of atmospheric turbulence and by various instrumental errors, and will be discussed in more detail in the next sections. This contribution does not depend on the stellar angular size to the first order.

3. ATMOSPHERIC TURBULENCE IN NULLING INTERFEROMETRY

Atmospheric turbulence induces two types of errors in a ground-based interferometer: phase errors, which can be divided into piston, dispersion and wavefront errors, and intensity errors. Both will reduce the ability of a nulling interferometer to cancel the stellar light with a high rejection rate. Another type of error affecting an interferometer is related to polarization effects. Polarization errors are however mainly due to instrumental imperfections rather than atmospheric turbulence, and will not be discussed here.

3.1. Effect of phase errors

3.1.1. Piston

The piston mode of turbulence corresponds to the fluctuations of the difference in average phase between the two apertures. It is produced by stochastic fluctuations of the refraction index of dry air, due to temperature and pressure fluctuations in the atmosphere. Piston induces an erratic movement of the central dark fringe in the transmission map, thereby degrading the nulling process as more stellar photons leak through the null. Since the refraction index of dry air is almost constant across the near- and mid-infrared, piston induces very little dispersion: the optical path difference (OPD hereafter) between the beams associated to the piston effect is almost wavelength-independent. The OPD fluctuations affecting the operation waveband of GENIE (L' band) could thus be controlled by measuring them in another waveband (e.g. at a shorter wavelength where more stellar photons are available).

The power spectrum of the fringe motion follows the classical Kolmogorov spectrum for atmospheric turbulence,[6] described by a power-law with a $-8/3$ slope. Due to correlations between the two apertures, the $-8/3$ slope for the power law is replaced by a $-2/3$ slope at frequencies below $f_1 \simeq 0.2\,v/b$ (with v the wind speed), while at frequencies higher than about $f_2 \simeq 0.3\,v/d$, pupil averaging changes the slope into $-17/3$. However, this latter slope has not been observed yet and will thus not be considered in the following discussion. The power spectrum of piston is illustrated in Fig. 2. Piston has a typical standard deviation of 20 μm rms. In the case of GENIE, this would completely ruin the nulling process because the rms fringe excursion is larger than the fringe spacing itself: the optical axis would therefore see both dark and bright fringes as atmospheric turbulence changes the phase difference between the apertures. Real-time OPD control by means of a fringe tracker is thus mandatory to improve the null depth N, which is related to the rms OPD error by the following relation[5]:

$$N \simeq \frac{4}{(2\pi\sigma_{\mathrm{OPD}}/\lambda)^2}\ , \tag{4}$$

valid for small OPD errors. In order to achieve a null depth of 10^5 required to detect 20-zodi disks, the rms OPD error should be less than about 4 nm, which is one to two orders of magnitude smaller than the performance achieved by current fringe tracking facilities.

3.1.2. Longitudinal dispersion

Unlike dry air, water vapor is highly dispersive in the near- and mid-infrared: its refraction index strongly depends on the wavelength. Therefore, it adds wavelength-dependence to OPD fluctuations as the column density of water vapor randomly fluctuates above the two telescopes. This effect, know as "longitudinal dispersion", can be divided into two contributions:

- *Inter-band dispersion.* This is the dispersion between the wavelength at which OPD control is performed and the wavelength at which the observation is done. If OPD control is done in the H band and the observation in the L' band, the typical standard deviation of dispersion-induced OPD is about 0.4 μm RMS, based of measurements of the water vapor column density fluctuations by Meisner and Le Poole.[7]

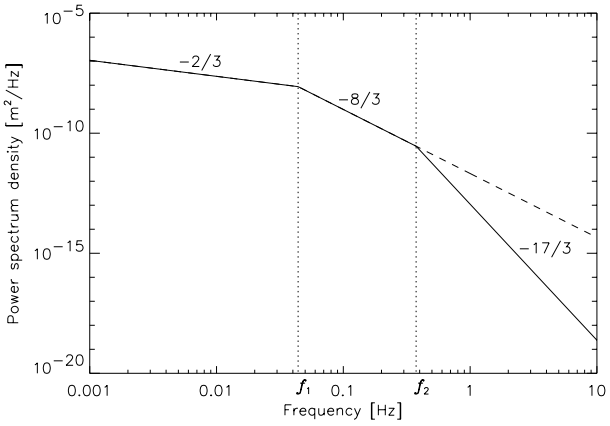

Figure 2. Differential piston power spectrum, under the following conditions: $B = 47$ m, $D = 8$ m, $v = 10$ m/s and $r_0 = 10$ cm at 500 nm. The effect of the outer scale of turbulence has not been included here. In the following discussion, pupil averaging is not be taken into account (dashed line).

- *Intra-band dispersion.* This is the dispersion inside the observation waveband itself: because of water-vapor dispersion, the OPD difference between the beams is not the same at the two edges of the observation waveband. The typical rms OPD difference between the two edges of the L' band (3.5 and 4.1 μm) is about 0.2 μm. These concepts are illustrated in Fig. 3.

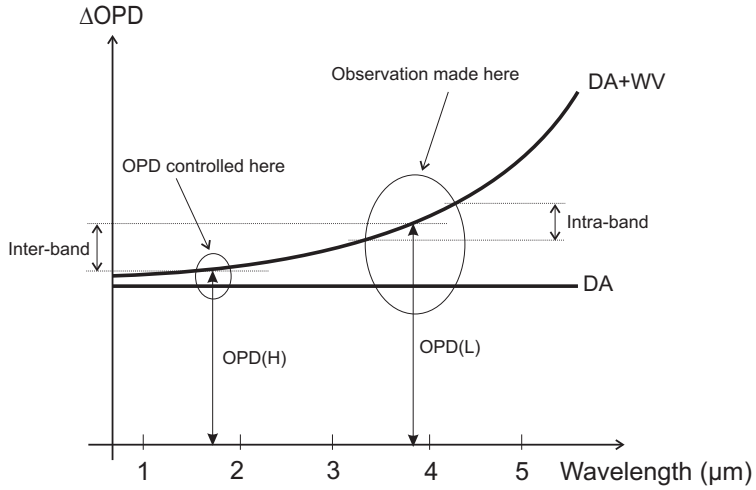

Figure 3. Illustration of inter-band and intra-band dispersion: the flat solid line is the rms differential OPD expected for only Dry Air, while the solid curve is the rms differential OPD in the presence of Water Vapor. Fringe tracking is supposed to be performed in the H band.

Both inter-band and intra-band dispersion need to be corrected in real-time in order to maintain a deep and stable nulling of the stellar light. Since dispersion control is not performed by the VLTI, a dedicated corrector will be included inside GENIE. Note that, unlike longitudinal dispersion, the effect of transverse dispersion (i.e., differential atmospheric refraction) on phase errors is almost negligible. Based on a code developed by E. Marchetti (see http://www.eso.org/gen-fac/pubs/astclim/lasilla/diffrefr.html), we have computed that the differential refraction is smaller than 100 mas between H and L' band. This is equivalent to a few millimeters over a distance of 10 km, barely the size of the smallest turbulent cells. Thus all wavelengths have undergone almost the same turbulent structure of the atmosphere, and their phase fluctuations are well correlated.

3.1.3. Wavefront errors

The quality of a wavefront is generally measured by its Strehl ratio, defined as the ratio of the on-axis intensity to that for a diffraction limited image. The Strehl ratio is also indicative of the amount of coherent energy in a given beam, i.e., the part of the beam that could interfere with another beam. At the VLTI, the UTs are equipped with a 60-actuator adaptive optics system (MACAO[8]) while two of the four planned ATs will be equipped with a tip-tilt corrector (STRAP). Both deliver a Strehl ratio of about 70% in the L' band, which means that 30% of the beam energy will not interfere at recombination and lead to an unacceptable additional stellar leakage. As shown by Mennesson et al.,[9] the use of modal filtering (e.g. using single-mode fibers) would allow to correct for both high and low order spatial frequencies, thereby ensuring a perfect matching of the amplitude profiles coming from the various beams over a broad bandwidth (typically an octave). The shape of the initial wavefront only affects the amount of energy coupled into the guide. The modal filter thus converts phase defects into intensity and piston errors, which are less severe for a nulling interferometer (see next section). In the following discussion, we assume that GENIE will be equipped with such modal filters.

3.2. Effect of intensity errors

The effect of intensity mismatches between the two beams of the interferometer is to produce an imperfect interference and thus to transmit some of the stellar light that should have been blocked. The main contributor to intensity mismatches between the beams of the interferometer is the fluctuation of the coupling efficiency into the single-mode waveguides. The coupling efficiency η relates to wavefront perturbations by the following relation[10]:

$$\eta \simeq \eta_0 \exp\left(-\sigma_\phi^2\right) \tag{5}$$

where σ_ϕ is the rms wavefront error expressed in radians and η_0 the coupling efficiency in absence of wavefront aberrations ($\eta_0 \simeq 79\%$ in the case of an UT with ideal injection conditions). For small phase aberrations ($\sigma_\phi < 2$ rad), the Strehl ratio can be approximated by $\exp(-\sigma_\phi^2)$. This is the case for GENIE since the VLTI provides a good wavefront correction through the MACAO adaptive optics system (on UTs) or the STRAP tip-tilt unit (on ATs), as illustrated in Table 1.

Table 1. Simulated rms tip-tilt, mean Strehl ratio (excluding tip-tilt) and rms Strehl ratio for an 8-m Unit Telescope after correction by MACAO, for an integration time of 2 sec.[2] A seeing angle $\alpha = 1$ arcsec is assumed.

	K	L'	N
Tip-tilt [mas]	13	13	13
$\langle S \rangle$	0.36	0.70	0.95
σ_S	0.063	0.044	0.008

The Strehl and tip-tilt fluctuations induce coupling fluctuations with a standard deviation as high as 10% of the mean coupled intensity. The nulling ratio associated to a relative intensity mismatch σ_I is given by[5]:

$$N \simeq 16/\sigma_I^2 \,, \tag{6}$$

so that an rms intensity mismatch of 10% induce a limitation of the nulling ratio of about 10^3, which is not sufficient to detect faint exozodiacal disks. Real-time intensity control is thus needed in order to meet the required nulling performance.

An additional contributor to intensity fluctuations is scintillation. Scintillation is the effect of rapid intensity fluctuations of a point-like source as a result of the interference of light rays which are diffracted by turbulent cells. The condition for scintillation to take place is that the light propagates through the atmosphere over distances longer than the Fresnel propagation length: $h \sec z \geq r_0^2/\lambda$, where h is the atmospheric scale height, z the zenithal angular distance and r_0 the Fried parameter.[11] With $r_0 \geq 5$ cm at $\lambda = 500$ nm and $r_0(\lambda) \propto \lambda^{6/5}$, we have $r_0^2/\lambda \geq 80$ km in the L' band, which is much larger than the atmospheric scale height. The condition for scintillation to appear is thus not satisfied in the mid-infrared and the effect of scintillation on intensity mismatches can be neglected.

4. CORRECTION OF ATMOSPHERIC EFFECTS

4.1. General scheme for a real-time control loop

Figure 4 represents the block-diagram of a general control loop. The input signal that has to be corrected is characterized by its Power Spectral Density (PSD) $S_{\rm in}$. A sensing unit (SU) measures the signal at a given repetition frequency. A certain amount of noise is produced by the detection: photon noise and read-out noise are the major contributions to the PSD of detection noise ($N_{\rm SU}$). The value measured by the sensing unit is then fed into a controller (K), which computes the correction to be applied. This process is supposed to be noise-free, but introduces some delay in the loop, referred to as "latency". The actuator (A), together with the Digital-to-Analog Converter, finally applies the relevant hardware correction to the input signal in order to compensate for the error. The actuation is not perfect; this is the reason why an amount of noise is added to the correction signal. The PSD of this noise source ($N_{\rm A}$) depends on the design of the actuator. It is not expected to be a dominant noise source. The performance of the control loop basically depends on the number of available photons at the sensing unit, which will determine the maximum repetition frequency at the which the sensor can operate and thus the maximum close-loop control bandwidth for the rejection of atmospheric turbulence.

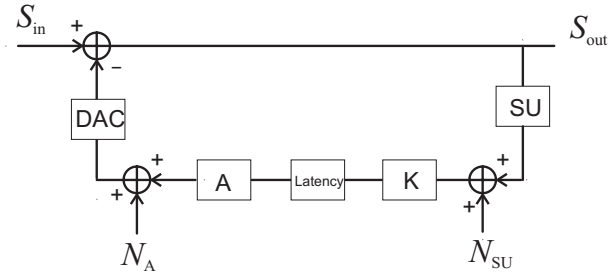

Figure 4. General scheme for a control loop.

In order to simulate the behaviour of the various control loops foreseen in GENIE, a software simulator for the GENIE instrument, called GENIEsim, has been developed at ESA/ESTEC.[3]

4.2. Real-time piston control

Piston correction can be done at any IR wavelength since piston is achromatic. A first stage of OPD control is provided by the PRIMA fringe sensing unit (operating in the K band) and the VLTI main delay lines. However, the correction accuracy (typically 150 nm rms on bright targets) is not sufficient for the GENIE purposes. Therefore, an additional stage of OPD control, with dedicated fast delay lines, will be implemented inside the GENIE instrument.

In order to meet the tight specifications on OPD control performance, the control loop should better operate at a wavelength where a large number of photons are available and a high signal-to-noise ratio achievable (i.e., small background emission). Control loop simulations with GENIEsim have shown that the H band is the most favorable band to perform high-precision OPD control. The correction will most probably be carried out by a fast delay line actuated by a piezo-translator operating up to a few tens of kHz. Assuming that all available H-band photons are used to feed the GENIE Fringe Sensor, that the loop can be runned at repetition frequencies up to 20 kHz with a latency below 10 μsec and that an optimal first order PID is used as OPD controller, the residual OPD after closed-loop control is about 4 nm RMS for typical GENIE targets (e.g. a G2V star at 10 pc). The PSDs at input and output of the GENIE OPD control loop are illustrated in Fig. 5.

4.3. Real-time dispersion control

Two kinds of corrections must be performed in order to control longitudinal dispersion:

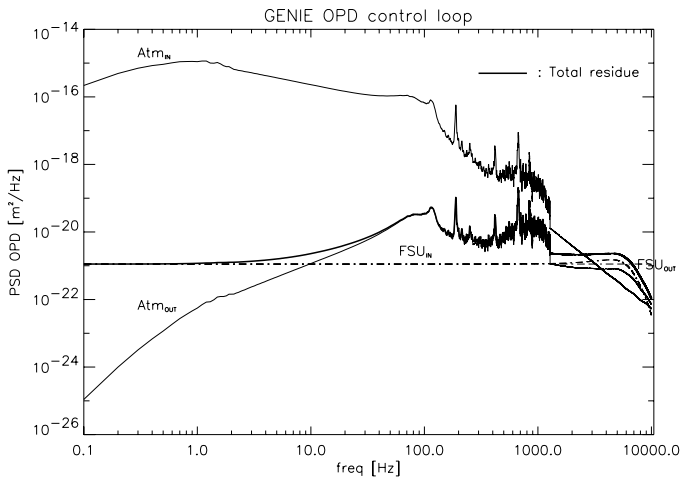

Figure 5. Power spectral densities (PSDs) of noise contributors in the GENIE OPD control loop. The input "atmospheric" PSD has already been partially corrected by the VLTI OPD control loop. The loop repetition frequency and the gain of the controller have been optimized so as to minimize the residual RMS OPD. The peaks between 200 and 1000 Hz are due to the piston mode of the MACAO deformable mirror.

- Inter-band dispersion correction, which co-phases the beams at the center of the observation waveband. There are two possible ways to operate the inter-band dispersion control loop: either by measuring directly the phase difference in the observation waveband, or by measuring the phase difference at two different wavelengths (outside the observation waveband) and then extrapolate (or interpolate) the dispersion curve towards the observation waveband to determine the actual phase difference in this band. This latter option is more risky since it relies on a model for the water vapor refraction index, which is of limited precision. Once it has been measured, inter-band dispersion can be corrected by means of a delay line, which can run at a lower frequency (of a few 100 Hz) than the previous one because dispersion is a smaller effect than piston (its rms is about 100 times less than the rms piston).
- Intra-band dispersion correction, which co-phases the beams across the whole observation waveband. As in the case of inter-band dispersion, the measurement can be made directly in the observation waveband or rely on extrapolation from measurement in other wavebands. In order to meet the specifications, both the first and second order dispersion terms should be corrected, requiring an actuator made up of two different dispersive materials with variable thickness (e.g. using wedges actuated by piezo translators). A stirrable pair of wedges made up of two different IR dispersive materials could thus be used both for achromatic phase shifting and dispersion correction at the same time.

Both corrections can thus rely on the same phase measurements obtained at two different wavelengths. The most robust solution would be to use the already recorded phase in the H band and then use an additional fringe sensor to measure the actual OPD in the L' band where GENIE operates. K-band photons could also be used to increase the precision in the phase measurement. Using K-band photons and 10% of the available L' band photons with repetition frequencies of about 100 Hz and an optimal first order PID controller, the residual inter- and intra-dispersion can be reduced below about 2 nm RMS for typical GENIE targets.

4.4. Real-time intensity control

The purpose of the intensity control loop is to equalize the intensities in the two beams of the interferometer, but not to stabilize the mean intensities in these two beams. At the output of the intensity control loop, the two beams will thus still fluctuate in intensity, but the two intensities will fluctuate in the same way. In order to perform the closed-loop correction, a part of the science beams will be diverted into "photometric channels", where the intensities of the beams will be measured. From these measurements, a controller will assess which one

of the beams has the highest intensity and feed the correction system with this information. The actuators should behave as similar as possible to a variable density filter in order to preserve the wavefront properties of the beams. Because of the high actuation frequency required (typically 1 kHz), a PZT-based actuator is recommended, e.g. a circular shutter with variable diameter. Simulations of the closed-loop performance of intensity matching show that a residual intensity mismatch of about 1% rms can be achieved on a Sun-like star at 10 pc.

5. PRELIMINARY DESIGN AND PERFORMANCE ESTIMATE FOR GENIE

In Fig. 6 is illustrated a possible design for the GENIE servo loops. All the actuators are placed before the sensors in order to perform closed-loop control. The signals recorded by the sensing units are treated by dedicated controller and then fed back to the actuators. Note that fibers are introduced in the photometric arms, because it must properly simulate the recombination conditions in the science beam (where fibers are used). Its is thus mandatory that the injection conditions for the photometric fibers are as close possible as for the science beams.

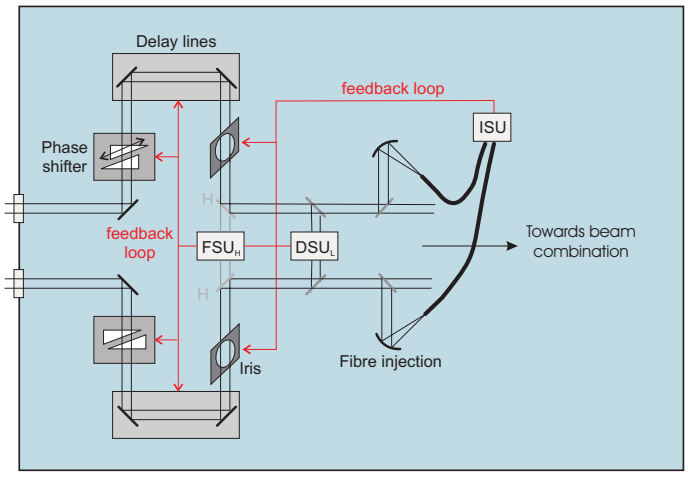

Figure 6. Architecture and preliminary design for the GENIE real-time servo loops. All the sensors (Fringe, Dispersion and Intensity Sensing Units) are located after the actuators in order to perform closed-loop control.

Using the GENIEsim simulation software, the performances of the GENIE servo loop systems have been estimated in the previous sections. They are summarized in Table 2, together with their equivalent null depth. From these individual contributors, we can deduce the overall null depth that can be achieved by GENIE. This table shows that null depths of typically 5×10^4 can be reached, which should allow to detect exozodiacal disks down to the 20-zodi level (for such disks, the initial star-cloud contrast is about 10^4 in the L' band). GENIE will thus allow to discard the inappropriate targets for the Darwin/TPF missions, i.e., the targets for which a large amount of circumstellar dust prevents from detecting possible Earth-like planets within a reasonable time.

Table 2. Expected performance of the GENIE servo loops, in terms of RMS residual perturbations, and associated null depth. The overall null depth that can be achieved by GENIE is deduced from these individual contributions.

	rms	null depth
OPD	4 nm	9.1×10^4
Dispersion	2 nm	3.7×10^4
Intensity	1%	1.6×10^5
Total		5.0×10^4

ACKNOWLEDGMENTS

O. A. acknowledges the financial support of the Belgian National Fund for Scientific Research.

REFERENCES

1. P. Gondoin, "Darwin-GENIE: a nulling instrument at the VLTI," in *New Frontiers in Stellar Interferometry*, W. Traub, J. Monnier, and M. Schoeller, eds., *Proc. SPIE* **5491**, 2004.
2. R. Wilhelm and P. Gitton, "The VLTI environment and GENIE," in *Toward Other Earths: Darwin/TPF and the Search for Extrasolar Terrestrial Planets*, **SP-539**, p. 659, ESA's Publication Division, 2003.
3. O. Absil, R. den Hartog, C. Erd, P. Gondoin, L. Kaltenegger, M. Fridlund, N. Rando, and R. Wilhelm, "GENIEsim: the GENIE simulation software," in *Toward Other Earths: Darwin/TPF and the Search for Extrasolar Terrestrial Planets*, **SP-539**, p. 317, ESA's Publication Division, 2003.
4. R. Bracewell, "Detecting nonsolar planets by spinning an infrared interferometer," *Nature* **274**, p. 780, 1978.
5. M. Ollivier, *Contribution à la recherche d'exoplanètes - Coronographie interférentielle pour la mission Darwin*. PhD thesis, Université de Paris XI, December 1999.
6. J.-M. Conan, G. Rousset, and P.-Y. Madec, "Wave-front temporal spectra in high-resolution imaging through turbulence," *J. Opt. Soc. Am. A* **12**(7), p. 1559, 1995.
7. J. Meisner and R. Le Poole, "Dispersion affecting the VLTI and 10 micron interferometry using MIDI," in *Interferometry in Optical Astronomy II*, W. Traub, ed., *Proc. SPIE* **4838**, pp. 609–624, 2003.
8. R. Arsenault, J. Alonso, H. Bonnet, J. Brynnel, B. Delabre, R. Donaldson, C. Dupuy, E. Fedrigo, J. Farinato, N. N. Hubin, L. Ivanescu, M. E. Kasper, J. Paufique, S. Rossi, S. Tordo, S. Stroebele, J. Lizon, P. Gigan, F. Delplancke, A. Silber, M. Quattri, and R. Reiss, "MACAO-VLTI: An Adaptive Optics system for the ESO VLT interferometer," in *Adaptive Optical System Technologies*, P. Wizinowich and D. Bonaccini, eds., *Proc. SPIE* **4839**, p. 174, 2003.
9. B. Mennesson, M. Ollivier, and C. Ruilier, "On the use of single-mode waveguides to correct the optical defects of a nulling interferometer," *J. Opt. Soc. Am. A* **19**(3), pp. 596–602, 2002.
10. C. Ruilier and F. Cassaing, "Coupling of large telescopes and single-mode waveguides: application to stellar interferometry," *J. Opt. Soc. Am. A.* **18**(1), pp. 143–149, 2001.
11. A. Quirrenbach, "Observing through the turbulent atmosphere," in *Principles of Long Baseline Stellar Interferometry*, P. Lawson, ed., pp. 71–86, JPL publ., 1999.